MM Science Journal | www.mmscience.eu
ISSN 1803-1269 (Print) | ISSN 1805-0476 (Online)
Special Issue | HSM 2023
17th International Conference on High Speed Machining
October 25-28, 2023, Nanjing, China
DOI: 10.17973/MMSJ.2023_11_2023102

HSM2023-00025

STUDY ON SURFACE INTEGRITY AND ITS INFLUENCE ON HIGH TEMPERATURE FATIGUE BEHAVIOR WHEN TURNING POWDER METALLURGY NI-BASED SUPERALLOY

Zheng MA[1], Jiaqiang DANG[1], Qi WANG[1,2], Weiwei MING[1]*, Qinglong AN[1], Ming CHEN[1]

[1] Shanghai Jiao Tong University, Shanghai 200240, School of Mechanical Engineering, Shanghai, PR China

[2] Changzhou Institute of Technology, Department of Aeronautics and Mechanical Engineering, ,Changzhou, PR China

*Corresponding author; e-mail: mingseas@sjtu.edu.cn

Abstract
As a member of the latest generation of powder metallurgy Ni-based superalloy, FGH96 has already been widely applied in the manufacturing of aero-engines because of its distinguished mechanical performances. The surface integrity plays an essential role in the final fatigue life of the machined parts. However, surface modification induced by the machining process is inevitable, which profoundly affects the high temperature fatigue behavior of the manufactured part during the service lifetime. To cover the gap, the present work was carried out to specially study the surface integrity and its influence on high temperature fatigue behavior of powder metallurgy Ni-based superalloy when subjected to the mechanical turning process. The surface integrity, including surface morphology, micro-hardness, and depth-dependent residual stress, was initially characterized under different input parameters. High temperature fatigue tests were then conducted on the processed specimens to correlate the surface integrity and its fatigue behavior. Results showed that input parameters greatly influence the surface condition and thus the high temperature fatigue behavior. Poor integrity on machined surface leads to poor fatigue performance with typical fatigue fracture morphology, including crack initiation, propagation, and final fracture. While fine integrity on machined surface contributes to better fatigue performance. More interestingly, the fracture morphology in this situation shows similarity to the static tensile fracture, which presents shear failure along the direction of maximum shear stress.

Keywords:
Ni-based superalloy, surface integrity, high temperature fatigue, high speed machining

1 INTRODUCTION

With the increasing demand of service performance in aero-engine, the turbine disk, as one of the essential components in aero-engine, raises its requirements on material property and manufacturing process [Haines 2022]. Comparing with other materials, powder metallurgy superalloy possesses advantages in many fields, such as the homogeneous formation, fine grain, high alloying degree, high temperature resistance, static strength, anti-fatigue performance [Shen 2022]. Therefore, powder metallurgy superalloy is commonly considered as the priority for manufacturing turbine disk in aero-engine [Norgren 2015].

As one of the latest generation of powder metallurgy Ni-based superalloys [Jithin 2022], FGH96 has already been widely applied in aero-engines because of its high strength, high temperature fatigue performance and creep resistance [Akhtar 2014]. Recently, a considerable amount of researches have grown up around the theme of FGH96 and its potential applications [Zhang 2013]. Researchers built a physically-based crystal slip model for creep deformation in FGH96, in order to estimate the impact of heat treatment on creep behavior in terms of γ' precipitate distributions [Peng 2016]. However, there still exists some shortcomings during the production process of FGH96 [Volpato 2022]. On the one hand, nonmetallic inclusions are inevitably mixed during the metallurgical process [Miao 2012]. On the other hand, typical surface defects, such as chip adhesion, feed mark, material debris, tears and cavities, are generated during the machining processes [Hu 2019]. Both kinds of defects greatly impact the high temperature fatigue performance as stress concentration points and potential crack initiations [Bijanzad 2021].

Therefore, it is of vital importance to study the fatigue performances of powder metallurgy superalloy at high temperature and correlate them with machining processes [Selvaraj 2021]. Wang et al. built a model to estimate the

fatigue performance of FGH96 and other superalloys by establishing relationships among fatigue strength co-efficient, ultimate strength, fatigue ductility coefficient, and percentage reduction of area. Comparing with the Four-Points Correlation Method, this method requires few testing points and also processes satisfactory results [Wang 2019]. Shi et al. investigated the fracture mechanism by exerting artificial crack-like defects on FGH96 specimens, which leads to a serious of life prediction methods with different strategies for surface cracks and stress concentrations [Shi 202]. Zhong et al. probed the influence of stress gradient on multiaxial fatigue life of FGH96 specimen. Comparing to six multiaxial models (the maximum effect strain model, the maximum shear strain model, the Fatemi-Socie model, the Smith-Watson-Topper model, the Itoh model, and the Zhong-Wang-Wei model), a modified Zhong-Wang-Wei model with stress gradient factor agrees better with the experimental results [Zhong 2018]. Zhang et al. captured the nucleation and evolution of fatigue damage in powder metallurgy Ni-based superalloy containing non-metallic inclusions by high resolution EBSD analysis [Zhang 2015].

In this paper, turning experiments were conducted on powder metallurgy Ni-based superalloy FGH96 initially. Through mechanical analysis of machining responses, specimens under typical parameter sets were selected for high temperature fatigue tests. Multiple characteristics, including surface roughness, hardness, residual stress and micro-morphology, were measured for the concern of surface integrity and its influence on the high temperature fatigue behavior. The present work aims to pro-vide guidance for the process optimization during the production of FGH96 parts.

2 MATERIALS AND METHODS

FGH96 is a type of powder metallurgy Ni-based superalloy with high proportion of γ phase, whose components are similar to RR1000, Alloy10, LSHR and René104. The powder of FGH96 is fabricated by plasma rotating electrode atomization (PREP) with particle sizes ranging from 50 μm to 150 μm. SEM and EDS was employed to capture the micro view of FGH96, as shown in Fig. 1. Mechanical properties of FGH96 is listed in Table 1.

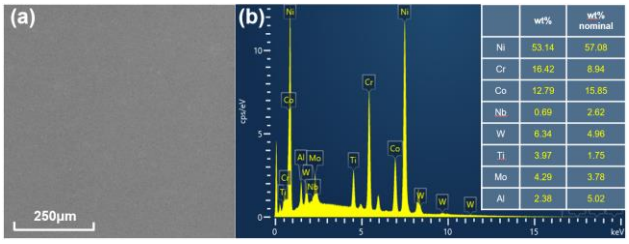

Fig. 1: (a) SEM and (b) EDS analysis of the powder metallurgy Ni-based superalloy FGH96.

Table 1: (a) SEM and (b) EDS analysis of the powder metallurgy Ni-based superalloy FGH96.

Tensile strength	Yield strength	Hardness	Density
1520 MPa	1200 MPa	6.73 GPa	9.2 g/m^3

Specimens of FGH96 were initially manufactured by the lathe ET3650 with different turning parameters. Resultant force was calculated by the equation:

$$F = \sqrt{F_p{}^2 + F_c{}^2 + F_f{}^2} \quad (1)$$

Where F_p , F_c and F_f represent the passive force, cutting force, feed force, and resultant (turning) force respectively.

High temperature fatigue tests are carried out on the test machine MTS809 (Mechanical Testing & Simulation Co., Ltd.) as shown in Fig. 2. The temperature maintains isothermal at 700℃ by the thermostat. Fatigue tests are controlled by strain as a ratio of R=0.05 and the maximum strain can reach 0.9% (alternating strain from compression to tension in axial direction periodically with the form of triangular wave). The loading frequency is 0.33 Hz. Fatigue tests terminate when specimens fracture.

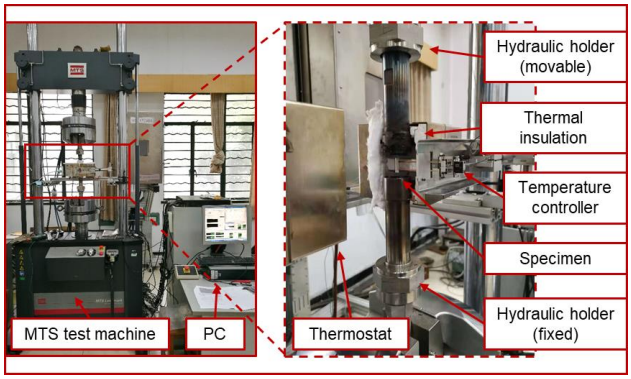

Fig. 2: Experimental setup for the high temperature fatigue test of FGH96.

3 RESULTS AND DISCUSSION

3.1 Analysis of machining response

Turning forces under different parameters were illustrated in Fig. 3, which were calculated from the stable turning process as root-mean-square values. Based on cutting orientation, cutting force occupies the largest share of resultant force and therefore dominates the trend of force changing with parameters. The increment of feed rate directly enlarges the cutting thickness, leading to the increase of the shear deformation zone. Since the resistance of shear deformation zone is the main source of force, it results in the increase of cutting force.

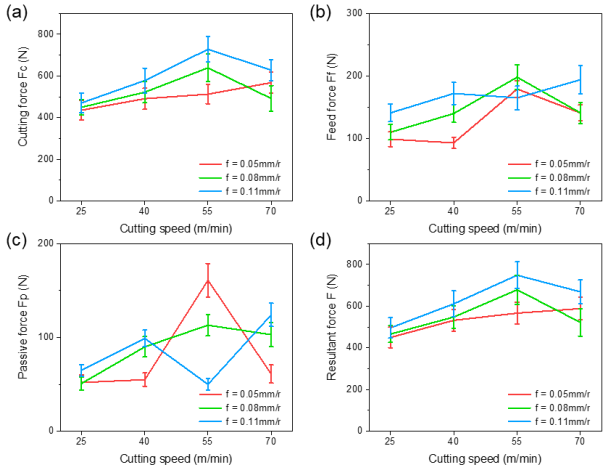

Fig. 3: Turning forces under different machining parameters

Turning temperatures under different machining parameters are illustrated in Fig. 4. The trend of turning temperature is not completely identical with the trend of turning force. Turning temperature increases with the cutting speed in general, since high speed causes severe friction and deformation.

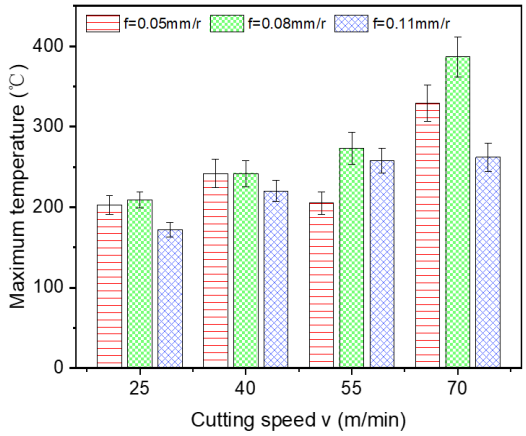

Fig. 4: Turning forces under different machining parameters

Surface roughness Ra, as shown in Fig. 5, is directly calculated from the surface morphology. With the increase of cutting speed, both axial and circular roughness increase first and then decrease. Maximum surface roughness reaches when cutting speed is 55m/min. The trend of surface roughness is similar to the trend of cutting force, indicating the positive correlation between force and surface roughness. Larger force induces severe wear and rough surface correspondingly. Taking turning force, temperature and surface roughness into consideration, heat-softening effect alleviates the turning condition when the cutting speed keeps increasing, leading to the improvement of turning force and surface roughness.

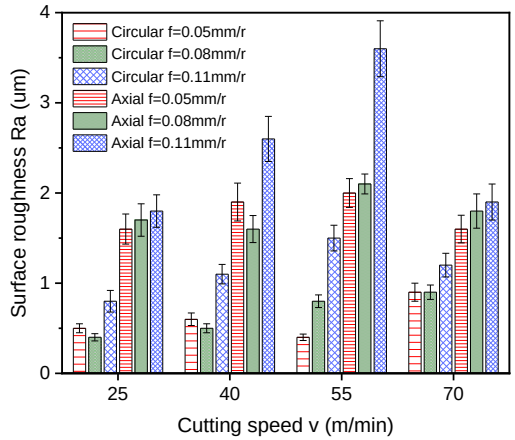

Fig. 5: Surface roughness under different machining parameters

3.2 Analysis of high temperature fatigue

Based on the analysis of machining responses, two sets of parameters are selected: v = 25m/min, f = 0.11 mm/r and v = 55m/min, f = 0.11 mm/r. According to IOS 1099 (Fig. 6 (a)), specimen is manufactured with these sets of parameters. For the convenience of writing, two sets of parameters are named as Set A and Set B, and each specimen are numbered, as shown in Fig. 6 (b). Generally, four specimens were manufactured for each set. Three of them (A/B-1, A/B-2, A/B-3) were employed on high temperature fatigue tests while the left one (A/B-4) was prepared for multiple measures, including metamorphic layer, surface hardness and residual stress.

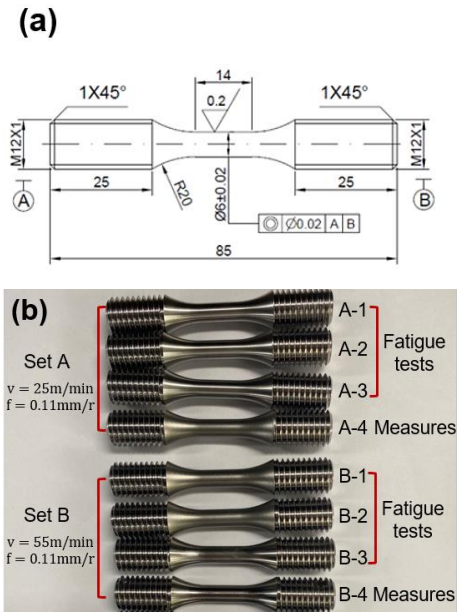

Fig. 6: Specimens of high temperature fatigue tests.

Metamorphic layers were filmed at a small piece cut in the normal direction (radial direction), as shown in Fig. 7. Generally, the surface area can be divided into three layers, work-hardening layer, mechanically and thermally affected layer, and reference layer, based on their metamorphic degrees. The work-hardening layer, locating at the top, is severely affected by the machining process, where dislocations and slips occupy compactly with the same orientation of feed rate. In the mechanically and thermally affected layer, the metamorphic degree is less severe than that of the work-hardening layer with the same orientation.

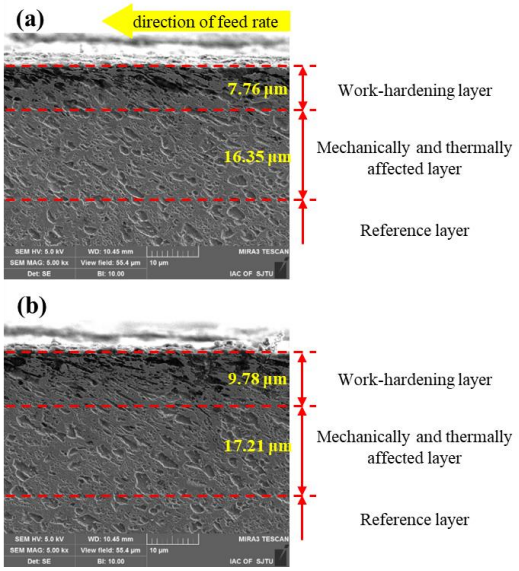

Fig. 7: Metamorphic layers of (a) Set A and (b) Set B.

Surface hardness was measured by the indentation tester, as shown in Fig. 8. Specially, five testing points are appointed on the radial section, which are spaced with a 5-μm interval. For each testing point, the value of hardness is calculated as the average of load-depth curve from 0 to 100 nm.

Conclusions can be summarized: 1) Work-hardening layer appears after turning process, which increases the hardness significantly. With the increase of depth, the hardness decreases after peak, and finally approaches to the value of matrix (6.73GPa). 2) The peak of Set B is approximately 50% larger than that of Set A. It can be inferred that the former work-hardening layer is affected more severely than the latter. 3) Taking Fig. 7 as reference, the average depth of work-hardening layer is consistent with the result of surface harness. It is reasonable to presume that the metamorphic layer of Set B is similar or slightly deeper than that of Set A.

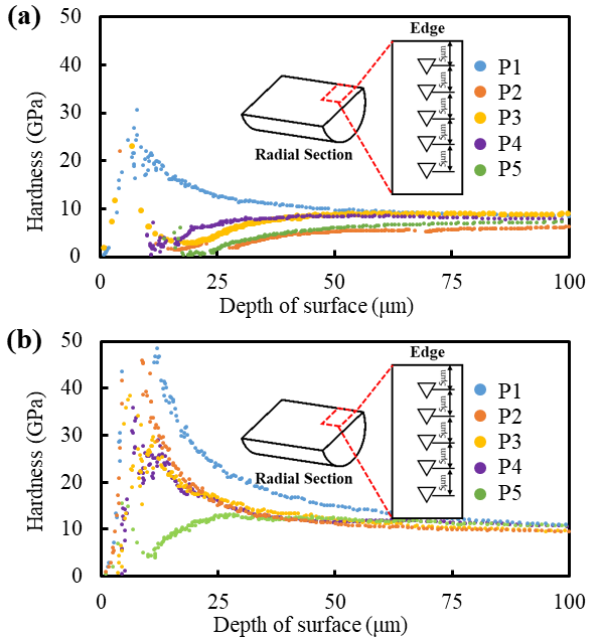

Fig. 8: Relationship between hardness and depth of surface of (a) Set A and (b) Set B.

Residual stress, as a function of depth, was measured both in axial and circular directions, as shown in Fig. 9. Residual stresses of machined surfaces are tensile in both axial and circular, whose values are relatively close to each other. In comparison, residual stress of Set A is slightly higher than that of Set B. It reveals that the impact of turning force on the residual stress is limited under these two sets. Combined with the analysis of metamorphic layer (Fig. 7), the trend of residual stress corresponds to the depth of metamorphic layer. When the depth is 30 μm, measuring results of residual stress are more likely to reflect the property of bulk material, since the measuring point at that depth is free from the influence of metamorphic layer. It reveals that the metamorphic layer, caused by turning process, is the key factor of residual stress. And it is sensible to estimate that the residual stress will not stop declining until it reaches the value of bulk material.

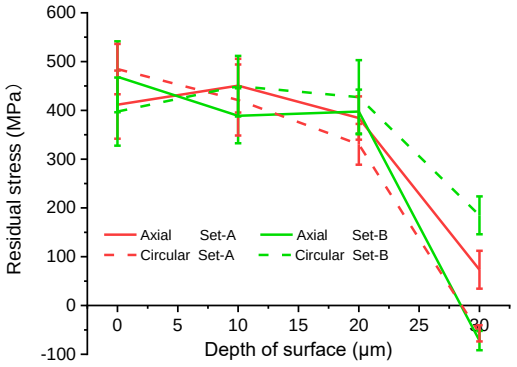

Fig. 9: Relationship between residual stress and depth of surface.

High temperature fatigue tests were conducted on specimens at 700℃, whose fatigue cycles are portrayed in Fig. 10. The average fatigue cycle of Set A are nearly three times than that of Set B. It can be inferred that the change of fatigue fracture mechanism is the key factor for the huge difference of fatigue cycle. Therefore, the following analysis lays emphasis on the morphology of fatigue fracture, in order to reveal the mechanism that conducts the fatigue behavior.

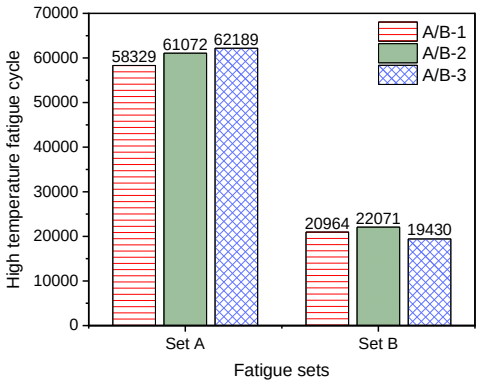

Fig. 10: Results of high temperature fatigue tests.

Fatigue fractures of specimens in each set share common characteristics. Therefore, it is reasonable to select specimens with middle fatigue cycle (A-2 and B-1) as representatives. Following analysis is established on these two specimens on behalf of each set.

The fatigue fracture of Set A, as in Fig. 11 (a), is similar to the static tensile fracture, which is featured by three regions (fiber-like region, propagation region and shear lip region). The fiber-like region is located at the center of the fracture, which is featured by the rough and fibrous morphology. The fiber-like region orients perpendicularly to the loading (axial) direction, known as the normal fracture. Cracks initiate at this region because of the cleavage under repeating loads. The propagation region surrounds the fiber-like region as a concentric annulus. It is considered as a symbol of transformation from slow crack initiation to fast crack propagation. The direction of crack propagation is marked by the radial divergence (radiating from inner to edge). In this case, the propagation region is not significantly bordered with other two adjacent regions, the fiber-like region at the center and the shear-lip region at the edge, because of the property of powder alloy. So the propagation region is not labeled in Fig. 11 (c). The shear-lip region appears at the final stage of the cracking process, which is featured by smooth surfaces and lip-like sections. Generally, this

region orients consistently with the direction of maximum shear stress (approximate 45° with the loading), known as the shear fracture. When the crack propagates beyond the limit, the unbroken part cannot bear the load and start to split within a short period, leaving 45°-oriented fracture and lip-like sections at edge. In other words, shear stress dominates the shear-lip region.

In order to reveal the detail morphology and its mechanism, high resolution SEM images of Set A are illustrated in Fig. 12. In a detailed view, the fiber-like region is featured mainly by cleavages and a small amount of dimples. Thus, it can be concluded that the crack initiation of Set A originates in the inner region. Under repeating loading, micro-cracks are formed at grain boundaries, phase boundaries and foreign inclusions. Cleavages are generated when micro-cracks propagate and tear up the matrix along grain boundaries. Dimples are generated when micro-cracks converge at a certain point. In the fiber-like region, the large amount of cleavages indicate that the crack propagation is slow at this period. The normal stress (along the direction of loading) dominates the crack propagation.

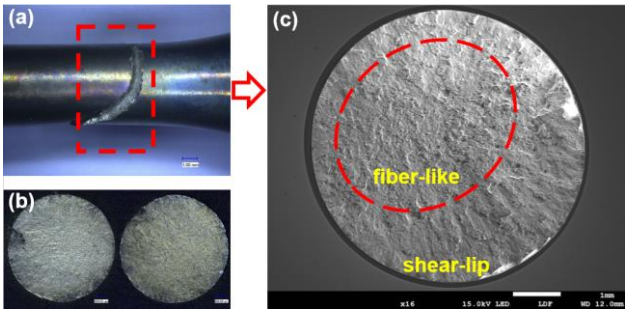

Fig. 11: Fracture morphology of Set A: (a) general view of fracture, (b) plan view of fracture section under optical microscope, (c) plan view of fracture section under SEM.

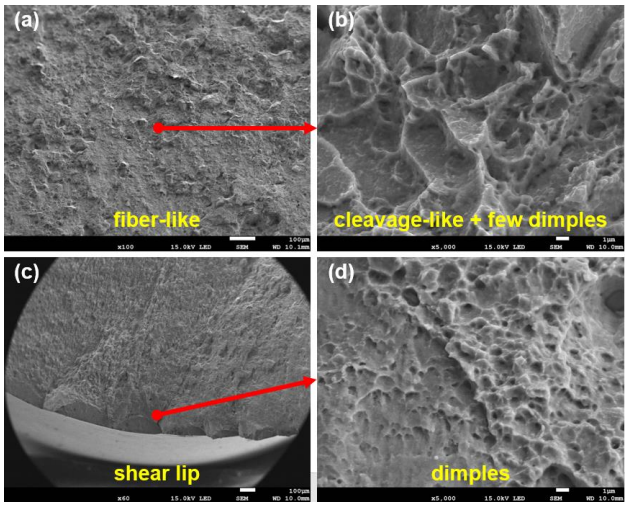

Fig. 12: Detailed view of Set A under SEM: (a) fracture morphology of the fiber-like region, (b) enlarged view of the marked area in the fiber-like region, (c) fracture morphology of the shear lip region, (d) enlarged view of the marked area in the shear lip region.

The fatigue fracture of Set B, as in Fig. 13 (a), is a typical case whose crack initiates at the edge. The crack initiation region, colored by oxidation in high temperature, is visible on the edge, which illustrates the crack initiation and expansion in early stage, as in Fig. 13 (b). Compared with the fracture of Set A, the crack location is deviated from the middle of specimen, which proves the attribution of surface initiation. From the macro view, the fracture can be divided distinctly into three regions: initiation region, propagation region, and final fracture region, as shown in Fig. 13 (c). Apparently, there are two initiations in this fracture. Crack initiation I contributes more than crack initiation II for the crack propagation based on their oxidation regions and trends in crack propagation. In both cases, the radiating divergence can be observed clearly from the initiation point. The surface of initiation region is relatively fine and smooth. Crack propagation starts at the initiation point and extends along the direction of slip band (from initiation point to interior). Generally, the propagation region is featured by cleavage-like planes, waving from the initiation region to the final fracture region. As for material with face-centered cubic (FCC) structure, like FGH96, the propagation is fully developed. In this case, the propagation region contains almost two thirds of the fracture area. The final fracture occurs when the crack propagates to a certain level and the remains cannot bear the external load. In this case, the final fracture region is a typical shear fracture with shear lip morphology, which orients consistently with the maximum shear stress (about 45° with the loading). Comparing with the shear lip region of Set A in Fig. 11 (a), the final fracture is small and limited in the peripheral area. The final fracture region is bordered with the propagation region clearly, indicating their difference in cracking mechanism. The propagation is a slow and periodic process while the final fracture is transient (within a cycle).

Similarly, high resolution SEM images of Set B are presented in Fig. 14, including two crack initiation regions, propagation region and final fracture region. Crack initiation I is characterized by scratch-like morphology, as shown in Fig. 14 (a). Since the orientation of crack initiation I is significantly different from the direction of crack propagation, it is reasonable to infer that crack initiation I belongs to surface defect during machining process. From Fig. 14 (b), the morphology of crack initiation II is distinct from that of the matrix material, which can be considered as foreign inclusions. From Fig. 14 (c), cleavages, a bunch of parallel strips with similar spacing, are observed clearly, whose orientation is perpendicular to the direction of crack propagation. Cleavages are formed by repeat loading. Each action of load drives the crack to propagate a step forward, leaving a parallel wave-like micro-cracks. From Fig. 14 (d), the final fracture region is occupied with dimples, where micro-cracks are formed by the shear stress during the crack propagation.

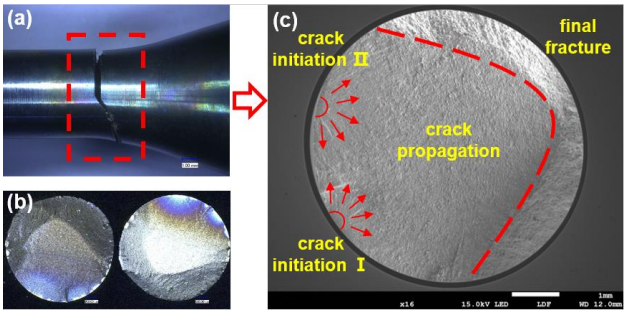

Fig. 13: Fracture morphology of Set B: (a) general view of fracture, (b) plan view of fracture section under optical microscope, (c) plan view of fracture section under SEM.

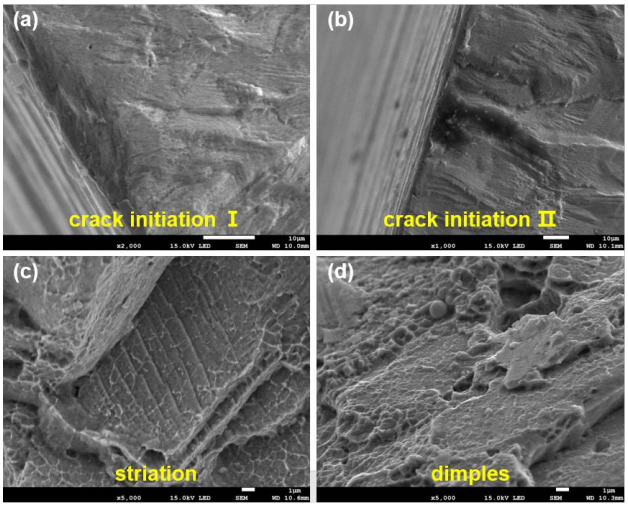

Fig. 14. Detailed view of Set B under SEM: (a) fracture morphology of the fiber-like region, (b) enlarged view of the marked area in the fiber-like region, (c) fracture morphology of the shear lip region, (d) enlarged view of the marked area in the shear lip region.

4 SUMMARY

In this study, typical machining parameters are set for the turning process of powder metallurgy Ni-based superalloy FGH96. And high temperature fatigue tests are carried out on specimens after turning. Conclusions can be summarized as follow:

(1) In the range of given parameters, turning force, surface roughness and tool wear show the same trend with cutting speed, which increase first and then decrease. Turning force is the key factor that dominates the machining response and the surface integrity.

(2) In the selected comparison of two parameters, Set A and Set B, turning force has a certain effect on the work-hardening layer and the surface hardness, but has no obvious effect on the surface residual stress. Compared with the results of fatigue cycle, however, turning force cannot produce a fundamental change in fatigue performance, in spite of exaggerating the metamorphic layer to some extent.

(3) Surface integrity is the key factor that dominates the high temperature performance of FGH96 specimen. Surface defect becomes the crack initiation in potential, which directly impacts the mechanism of fatigue fracture, and therefore affects the fatigue performance.

(4) Two models of fracture mechanism were cataloged with direct relation of the surface integrity. When the defect is located at the surface or subsurface, the fracture morphology is featured by the typical fatigue cracking with crack initiation, crack propagation and final fracture. When the crack starts at the core, the fracture morphology is similar to that of static tensile fracture, which is composed of fiber-like region, propagation region, and shear-lip region. Apparently, the fatigue performance of the former is poorer than the latter.

(5) Two types of crack initiations are found at the surface of specimen. One belongs to the machining defect, and another one belongs to the metallurgical inclusion. The former affects the high temperature fatigue performance far more than the latter. Therefore, it is helpful to improve the high temperature fatigue property by optimization of machining process and control of surface defects.

5 ACKNOWLEDGMENTS

The work is supported by National Natural Science Foundation of China (No. 92160206), Shanghai Industrial Collaborative Innovation Project (Grant No. HCXBCY-2022-040), Project of Changzhou Basic Research Program (No. CJ20220239) and General Program of Basic Science of Higher Education of Jiangsu (No. 22KJB460014).

6 REFERENCES

[Akhtar 2014] Akhtar W., et al. Tool wear mechanisms in the machining of Nickel based super-alloys: A review. Frontiers of Mechanical Engineering, 2014, 9(2): 106-119. ISSN 20950233.

[Bijanzad 2021] Bijanzad A., et al. Heat-assisted machining of superalloys: a review. The International Journal of Advanced Manufacturing Technology, 2021, 118(11-12): 3531-3557. ISSN 02683768.

[Haines 2022] Haines M. P., et al. Powder bed fusion additive manufacturing of Ni-based superalloys: a review of the main microstructural constituents and characterization techniques. Journal of Materials Science, 2022, 57(30): 14135-14187. ISSN 00222461.

[Hu 2019] Hu D., et al. Effect of inclusions on low cycle fatigue lifetime in a powder metallurgy nickel-based superalloy FGH96. International Journal of Fatigue, 2019, 118: 237-248. ISSN 01421123.

[Jithin 2022] Jithin S. D., et al. Comparative Analysis between 5th and 6th Generation Superalloys and Previous Generation Superalloys. Advances in Materials Science and Engineering, 2022, 2022: 1-21. ISSN 16878442.

[Miao 2012] Miao J., et al. Microstructural extremes and the transition from fatigue crack initiation to small crack growth in a polycrystalline nickel-base superalloy. Acta Materialia, 2012, 60(6-7): 2840-2854. ISSN 13596454.

[Norgren 2015] Norgren S., et al. Trends in the P/M hard metal industry. International Journal of Refractory Metals and Hard Materials, 2015, 48: 31-45. ISSN 02634368.

[Peng 2016] Peng Z., et al. Mechanistic behaviour and modelling of creep in powder metallurgy FGH96 nickel superalloy. Materials Science and Engineering: A, 2016, 676: 441-449. ISSN 09215093.

[Selvaraj 2021] Selvaraj S. K., et al. Recent Advancements in the Field of Ni-Based Superalloys. Advances in Materials Science and Engineering, 2021, 2021: 1-60. ISSN 16878442.

[Shen 2022] Shen J., et al. Thermomechanical fatigue behavior and lifetime modeling of powder metallurgy superalloy considering phase angle effect. International Journal of Fatigue, 2022, 164. ISSN 01421123.

[Shi 2020] Shi Y, Yang X, Yang D, Shi D, Miao G, Wang Z. Evaluation of the influence of surface crack-like defects on fatigue life for a P/M nickel-based superalloy FGH96. International Journal of Fatigue, 2020, 137. ISSN 01421123.

[Volpato 2022] Volpato G. M., et al. A comprehensive literature review on laser powder bed fusion of Inconel superalloys. Additive Manufacturing, 2022, 55. ISSN 20754701.

[Wang 2019] Wang Y., et al. Estimation of fatigue parameters in total strain life equation for powder metallurgy superalloy FGH96 and other metallic materials. International Journal of Fatigue, 2019, 122: 116-124. ISSN 01421123.

[Zhang 2013] Zhang M., et al. Effect of heat treatment on the micro-indentation behavior of powder metallurgy nickel based superalloy FGH96. Materials & Design, 2013, 49: 705-715. ISSN 02613069.

[Zhang 2015] Zhang T., et al. Slip localization and fatigue crack nucleation near a non-metallic inclusion in polycrystalline nickel-based superalloy. Materials Science and Engineering: A, 2015, 641: 328-339. ISSN 09215093.

[Zhong 2018] Zhong B., et al. Multiaxial fatigue life prediction for powder metallurgy superalloy FGH96 based on stress gradient effect. International Journal of Fatigue, 2018, 109: 26-36. ISSN 01421123.